Journal of Solid State Chemistry 184 (2011) 3040–3049

Contents lists available at SciVerse ScienceDirect

Journal of Solid State Chemistry

journal homepage: www.elsevier.com/locate/jssc

# Structural and electronic evolution of $Cr_2O_3$ on compression to 55 GPa

Przemyslaw Dera [a,*], Barbara Lavina [b], Yue Meng [c], Vitali B. Prakapenka [a]

[a] Center for Advanced Radiation Sources, The University of Chicago, Argonne National Laboratory, Building 434A, 9700 South Cass Ave., Argonne, IL 60439, USA
[b] High Pressure Science and Engineering Center and Department of Physics and Astronomy, University of Nevada, Las Vegas, NV 89154, USA
[c] HPCAT, Geophysical Laboratory, Carnegie Institution of Washington, 9700 South Cass Avenue, Argonne, IL 60439, USA

ARTICLE INFO

*Article history:*
Received 18 August 2011
Received in revised form
12 September 2011
Accepted 14 September 2011
Available online 21 September 2011

*Keywords:*
High pressure
Phase transitions
Optical absorption
Corundum
Ruby
Eskolaite

ABSTRACT

Synchrotron single-crystal x-ray diffraction experiments have been performed on corundum-type $Cr_2O_3$ up to a pressure of 55 GPa in Ne and He pressure transmitting media. Diffraction experiments were complemented by measurements of optical absorption spectra with single crystal samples up to 60 GPa. Results of the diffraction data analysis rule out the earlier reported monoclinic distortion at 15–30 GPa, but indicate evidence of two discontinuous transitions of electronic or magnetic nature, most likely associated with a change in magnetic ordering and charge transfer. The compression mechanism established from single crystal refinements indicates much smaller distortion of the $Cr^{3+}$ coordination environment than was previously assumed.



## 1. Introduction

The corundum structure is adopted by a wide class of inorganic crystalline materials, many of which have significant technological applications in the ceramic industry as abrasives, in optics, and in electronics, including fabrication of superconducting devices, complementary metal oxide semiconductor (CMOS) and possibly magnetoresistive random access memory (MRAM). Ruby, $(Al,Cr)_2O_3$ has been the basis of the most widely used pressure calibration scale for in situ diamond anvil cell studies for several decades [1,2]. Corundum, and closely related ilmenite structure minerals, also play important roles in the geology of the deep Earth interior. Because of these applications, understanding of the structural mechanism of compression, response to stress, as well as phase transformations in corundum type oxides are of great interest both from the basic, as well as applied science perspectives.

The high-pressure behavior of eskolaite, the Cr-end member of the $(Cr,Al)_2O_3$ solid solution, has been an object of active investigation for the last half century. In addition to early studies [3–5], three recent experiments attempted to constrain the structural evolution and phase diagram of $Cr_2O_3$ at high pressure. Rekhi et al. [6] used a custom laboratory XRD instrument and performed cold compression (at ambient temperature) experiments with polycrystalline $Cr_2O_3$ in an alcohol pressure medium with Ag pressure standard to 30 GPa. No phase transition was detected to the highest pressure reached. Moguin et al. [7] used synchrotron powder XRD and Raman spectroscopy in silicon oil, as well as Ar pressure media, and conducted a cold compression experiment to 50 GPa. Again, no phase change was detected to 25 GPa, however, the powder patterns at higher pressure could not be reliably fit with the corundum structure model. Most recently Shim et al. [8] used synchrotron powder diffraction and Raman spectroscopy and conducted compression experiments to 62 GPa including laser heating of the sample at 30 GPa. Based on the combined spectroscopic and diffraction evidence a monoclinic distortion of the ambient, rhombohedral structure, similar to a distortion occurring in $V_2O_3$ at low temperature [9] was suggested above 15 GPa, and an orthorhombic phase was detected after heating at 30 GPa [8]. These findings brought new and important information about the compression behavior and electronic transformations of α-chromia, however, the available evidence, due to intrinsic limitations of the experimental methods used, has not been entirely conclusive.

At ambient conditions the corundum-type $Cr_2O_3$ phase is an antiferromagnetic insulator (AF1) with Néel temperature $T_N = 311.5$ K, above which a transition to a paramagnetic insulating state (PM) occurs [10]. Some controversy exists in the literature, regarding both the value, as well as the sign of the pressure derivative of $T_N$. Magnetoelectric susceptibility disappearance, [11] points to a $\partial T_N/\partial p > 0$, whereas disappearance of coherent magnetic scattering in neutron diffraction suggests

* Corresponding author.
*E-mail address:* dera@cars.uchicago.edu (P. Dera).

0022-4596/$ - see front matter © 2011 Elsevier Inc. All rights reserved.
doi:10.1016/j.jssc.2011.09.021

$\partial T_N/\partial p < 0$ [10]. With negative $\partial T_N/\partial p$ $Cr_2O_3$ would be a paramagnet at ambient temperature and pressure of few GPa, whereas positive $\partial T_N/\partial p$ would preserve the antiferromagnetic ordering to much higher pressures.

First principles calculations have been carried out to consider other possible magnetic structures, as well as their evolution on compression. Catti et al. [12] considered three different antiferromagnetic states (AF1, AF2, AF3) and a ferromagnetic state (FM), and demonstrated that within the unrestricted Hartree–Fock approximation, the ground state at ambient pressure should be antiferromagnetic with $+-+-$ spin (AF1) configuration. More recent calculations in local spin density approximation[13] with AF1, FM and paramagnetic (PM) configurations suggest that all three magnetic states should exhibit a distinct compression behavior of the *c/a* ratio.

Powder x-ray diffraction at pressures above 20 GPa with quasi-hydrostatic pressure media such as Ar suffers from significant problems with uniaxial-stress-related peak broadening, preferred orientation, as well as peak overlaps of sample and pressure medium peaks. This results in a very limited resolving power for subtle structural distortions, such as the $R\text{-}3c \rightarrow I2/a$ transition suggested to take place in $Cr_2O_3$ at high pressure [8]. Diffraction experiments with single crystal samples, on the other hand, offer a far superior level of details regarding low symmetry distortions and provide the possibility to reliably resolve similar but crystallogrphically distinct structures. However, thus far, with few very recent exceptions, single crystal experiments have been limited to pressures not exceeding 15 GPa. Equipped with a combination of the synchrotron single crystal x-ray diffraction technique recently implemented at Sectors 13 and 16, Advanced Photon Source, Argonne National Laboratory, and optical absorption spectroscopy we decided to conduct a detailed study of the structural and electronic evolution of synthetic $Cr_2O_3$ at high pressure, aiming to resolve the enigma of the monoclinic distortion.

## 2. Experimental

### 2.1. Diffraction

Two independent experiments, S1 and S2 were conducted. In both experiments diamond anvils with 0.3 mm culet size and Re gasket preindented to a thickness of approximately 0.04 mm were used. A combination of backing plates made of cubic boron nitride (towards the incident beam) and Boehler/ALMAX design (towards the detector) was used to maximize the angular access to the sample. Experiment S1 was carried out at the GSECARS facility at APS, Argonne National Laboratory, in experimental station 13IDD. A monochromatic beam with an incident energy of 37 keV, focused with a pair of Kirkpatric-Baez mirrors to a spot of 0.003 by 0.005 mm was used. Diffraction images were collected using a MAR165 charge coupled device (CCD) detector, placed at a sample-to-detector distance of approximately 200 mm. During the exposure the sample was rotated about the vertical axis of the instrument ($\omega$) in the range of 50°, with a typical exposure time of 0.5 s/degree. Diffraction images were collected at three different detector positions, differing by a translation of 70 mm perpendicular to the incident beam. The detector geometry parameters at each detector position were calibrated with a $CeO_2$ NIST diffraction standard. In addition to the full-rotation exposures, a step-scan with 1° rotation steps was performed at each pressure step, for each of the sample crystals. Three microcrystals of synthetic $Cr_2O_3$ (Alfa Aesar, #10688, 99.97% purity) with different orientations and approximate sizes of $0.020 \times 0.010 \times 0.005$ mm$^3$ were loaded into a diamond anvil cell (DAC). The gasket hole with initial diameter of 0.180 mm was filled with Ne as the pressure medium, using the GSECARS/COMPRES gas loading apparatus [14]. After filling the DAC with Ne the gasket hole diameter decreased to 0.080 mm and remained unchanged to the highest pressure reached. The samples were compressed to 55 GPa in approximately 5 GPa pressure steps, with full SXD data collection at each step. Diffraction images were analyzed using the GSE_ADA/RSV software package [15]. The samples, which were initially semitransparent green, went through two discontinuous color changes on compression to 55 GPa. First, at around 13 GPa, the previously reported [8] change from green to red was observed, while at about 30 GPa a new change, from red to orange was found. No indication of monoclinic distortion was found in the x-ray diffraction data throughout the entire pressure range covered in experiment S1.

The quality of the diffraction data in experiment S1 gradually deteriorated, and at the highest pressure quite significant peak broadening was observed, as illustrated in Fig. 1. It should be emphasized that such strong peak broadening is not typical for single-crystals in Ne (e.g. no similar peak broadening was observed in our experiments with single-crystal $Fe_2O_3$ in Ne at similar pressure), and in $Cr_2O_3$ it seems to be related to some intrinsic microstructural effects. Klotz et al. [16] recently examined the degree of departure from ideal hydrostaticity in Ar, Ne and He pressure media, which was quantified by means of standard deviation $\sigma$ of the value of pressure determined from an array of multiple ruby spheres placed in the same diamond anvil cell. At 30 GPa the values of $\sigma$ for Ar, Ne, and He were 0.7, 0.25, and 0.11 GPa, respectively, indicating, that the Ar medium produces much larger stress anisotropy than Ne and He, but even Ne is about two times more nonhydrostatic than He.

To further confirm the observations made in experiment S1, as well as to assess the role of uniaxial stress, we conducted a second single-crystal synchrotron diffraction experiment, S2 using two microcrystals of $Cr_2O_3$ of the same origin as the sample in experiment S1 and He pressure transmitting medium. The diffraction experiment was carried out at the HPCAT facility at APS, Argonne National Laboratory in the experimental station 16IDB. In experiment S2 a monochromatic beam with an incident energy of 30 keV, focused with a pair of Kirkpatric-Baez mirrors to a spot of 0.005 by 0.008 mm was used. The instrument configuration and data collection strategy were analogous as in experiment S1. Thanks to the use of the softer He medium the quality of diffraction data in this experiment remained very high up to 55 GPa and diffraction peak profiles remained sharp, as illustrated in Fig. 1. In all the experiments pressure was determined by the ruby fluorescence method [1]. In all the experiments the diameter of the ruby spheres was chosen to be slightly larger than the thickness of the crystals to provide easily identifiable indication of possible sample bridging between the diamonds (bridging of the ruby sphere would be observed first, and would be indicated by broadening of the fluorescence lines). No signature of bridging was observed in either of the experiments.

### 2.2. Unit cell refinement and structure determination

Unit cell parameters were calculated at each pressure step using the GSE_ADA/RSV software, based on the diffraction peak d-spacings, with trigonal constraints. Unconstrained refinements carried out at each pressure step did not indicate significant departures from the trigonal symmetry throughout the whole pressure range studied. Data from all sample crystals contained in the DACs were merged together to increase precision of the unit cell parameter determination. In experiment S1 the total number of peaks used for unit cell parameter refinement varied from 554 at 1.62 GPa to 274 at 55 GPa (because of the peak broadening at increasing pressure the total number of peaks observed

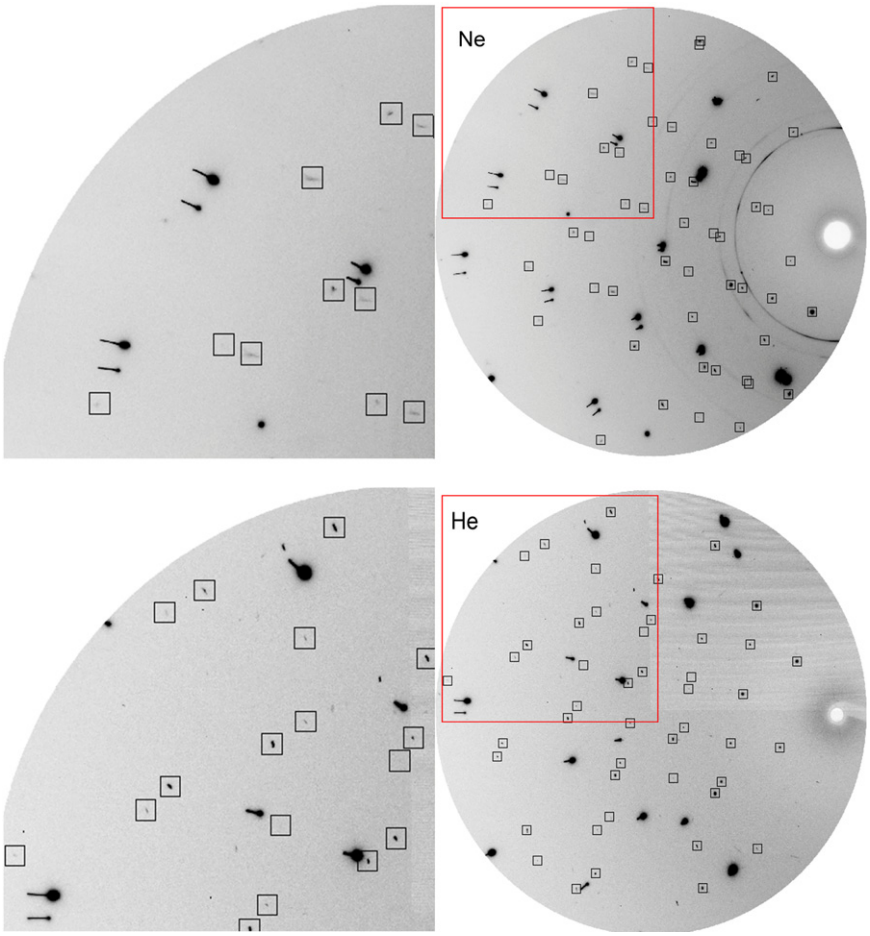


**Fig. 1.** Single-crystal diffraction patterns of $Cr_2O_3$ at 55 GPa from experiment S1 in Ne medium (top) and S2 in He medium (bottom). Some of the diffraction peaks from the sample in Ne show significant broadening.

decreased). In experiment S2 data from just one of the crystals were used for refinement, which resulted in 148 peaks at 4.53 GPa and 131 peaks at 55.18 GPa.

Integrated peak intensities were fit using the GSE_ADA program, and corrected for DAC absorption, Lorenz and polarization effects. Because of the high incident energy and negligible sample thickness, sample absorption was ignored. Peaks from exposures at the three different detector positions were scaled and merged together. The resulting lists of peaks with corresponding squares of structure factor amplitudes $|F|^2$ and their standard deviations were used for structure refinement. All refinements were carried out using the SHELXL program [17]. The refinements were done using anisotropic displacement parameters for both atoms.

### 2.3. Optical absorption spectroscopy

A symmetric DAC equipped with type Ia diamonds with 0.250 mm culets and Re gasket, preindented to initial thickness of 0.035 mm was used. The sample was an unpolished fragment with a flat platelet shape and uniform thickness, with approximate size $0.025 \times 0.025 \times 0.003$ mm$^3$. The crystal was oriented with the [0 1 2] vector approximately normal to the flat surface. A small ruby sphere was loaded together with the sample crystal to provide a pressure reference scale. Ne was used as the pressure transmitting medium.

A modified Raman spectrometer with standard tungsten filament lamp illuminator unpolarized light source was used for collection of the absorption spectra. The experimental setup utilized SPEX HP460 double grating monochromator and a liquid $N_2$-cooled ST-133 CCD detector. The spectra were collected using a 300 grating, in four spectral ranges, centered at 420, 600, 780 and 900 nm and scaled together. A typical acquisition time for each spectrum was 5 s. A $20 \times 20$ mm$^2$ motorized slit was used to define the region inside the DAC gasket hole through which the light was passed.

## 3. Results and discussion

### 3.1. Monoclinic phase

To our knowledge pure and up to 4% Cr-doped $V_2O_3$ are the only known transition metal oxide (TMO) systems that have been demonstrated to undergo the monoclinic distortion of the corundum structure at low temperature [18,19]. The monoclinic distortion has never been shown to occur as a function of pressure. $Al_2O_3$ and $Fe_2O_3$, the two TMOs most extensively studied at high pressure, transform directly from the hexagonal to orthorhombic structures. In $V_2O_3$ the deformation of the hexagonal symmetry accompanying the low temperature phase transition is quite significant [9]. The effect of doping the $V_2O_3$ structure with small amount of Cr gradually diminishes the magnitude of the effect [18], and by extrapolation to the pure Cr system it should be expected that the monoclinic phase would not occur in pure $Cr_2O_3$. Furthermore, even in the pure $V_2O_3$ system the $T_c$ of the metal-to-insulator transition falls to 0 K at

pressures below 2 GPa, and the monoclinic distortion is suppressed above this pressure [20].

Monoclinic distortion can be detected in single crystal experiments in several ways: (i) the unit cell parameters, refined both on the basis of peak d-spacings, as well as inter reciprocal vector angles deviate from the ideal hexagonal values (e.g. in case of the temperature-driven transition in $V_2O_3$ the monoclinic angle departs from 90° by more than 1 degree) [9] (ii) intensities of peaks equivalent in hexagonal structure no longer agree with each other, leading to increase of the peak intensity internal consistency factor $R_{int}$ and (iii) the hexagonal structure model is no longer appropriate to describe the distorted structure, resulting in the increase of refinement reliability factor $R_1$. In the particular case of a single-crystal sample and the monoclinic distortion occurring in $V_2O_3$ at low temperature, there should be an additional indication of the transformation, as the single-crystal peaks should split due to formation of monoclinic twin domains [9].

In our single-crystal data up to 55 GPa none of the above distortion-indicating criteria were satisfied, suggesting that the structure retains the original, rhombohedral symmetry. In both experiments S1 and S2 structure refinement conducted in the $R\bar{3}c$ space group yielded very good agreement of calculated and experimental peak intensities, as summarized in Tables 1 and 2.

### 3.2. Compression mechanism

In the corundum structures the metal $M^{3+}$ cations are located in octahedral coordination. Only two fractional atomic coordinates, $Z_M$ and $X_O$ are needed to fully describe the corundum structure, with the Cr and O atoms located at special positions with coordinates 0, 0, $Z_M$ (12*c* Wyckoff position) and $X_O$, 0, 1/4 (18*e* Wyckoff position), respectively. Each $CrO_6$ octahedron shares one face and three edges with neighboring occupied octahedra, as shown in Fig. 2. At ambient pressure the cation is slightly displaced from the geometric center of the coordination octahedron, to minimize the electrostatic repulsion across the shared face. As a consequence of this displacement the three *M*–O bonds to the face-shared oxygen atoms (Cr–$O_s$) are slightly longer than the remaining three bonds (Cr–$O_u$). Three different classes of short O–O contacts can be distinguished: shortest, involved in the shared octahedral face (O–$O_{SF}$), intermediate, involved in the shared edge (O–$O_{SE}$) and longest, involved only in the corner-sharing (O–$O_{CS}$).

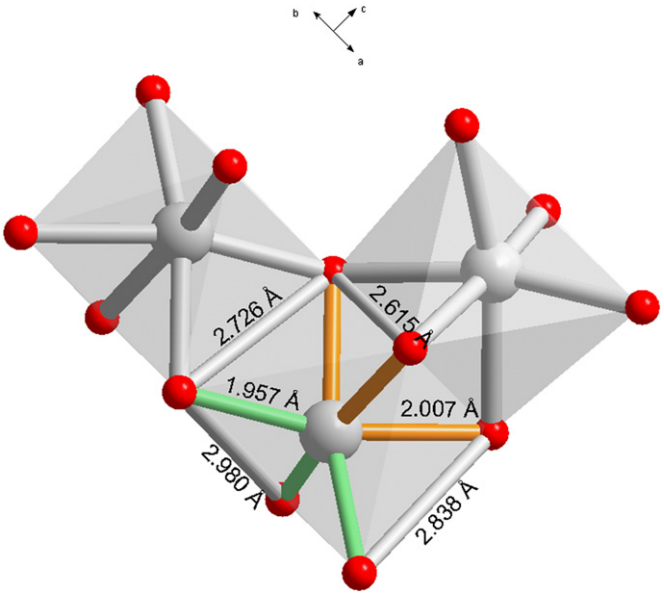


**Fig. 2.** Coordination environment of $Cr^{3+}$ at 1.62 GPa (from experiment S1 in Ne medium).

**Table 1**
Crystal data and structure refinement at selected pressure points parameters in experiment S1 ($\lambda$=0.3344 Å) in Ne medium.

| | | | | | | |
|---|---|---|---|---|---|---|
| Pressure (GPa) | 3.62 | 11.80 | 19.04 | 29.32 | 35.34 | 41.05 |
| Unit cell parameters (Å) | *a*=4.9300(4) *c*=13.507(1) | *a*=4.8789(4) *c*=13.372(2) | *a*=4.8330(7) *c*=13.254(2) | *a*=4.7803(7) *c*=13.139(3) | *a*=4.7521(9) *c*=13.080(4) | *a*=4.726(1) *c*=13.033(5) |
| Reflections collected/unique | 216/72 [R(int)=0.141] | 207/77 [R(int)=0.131] | 157/66 [R(int)=0.128] | 173/71 [R(int)=0.144] | 156/65 [R(int)=0.186] | 117/58 [R(int)=0.147] |
| Theta range (deg.) | 2.66 to 17.86 | 2.68 to 17.94 | 2.71 to 18.12 | 4.01 to 18.06 | 4.04 to 17.30 | 3.34 to 17.84 |
| Completeness to max. theta (%) | 34.8 | 37.7 | 32.4 | 36.0 | 37.4 | 33.3 |
| Data/restraints/parameters | 72/0/9 | 77/0/9 | 66/0/9 | 71/0/9 | 65/0/9 | 58/0/9 |
| Goodness-of-fit on $F^2$ | 1.216 | 1.243 | 1.150 | 1.082 | 1.253 | 0.900 |
| Final *R* indices (all data) | *R*1=0.0669, *wR*2=0.1609 | *R*1=0.0566, *wR*2=0.1406 | *R*1=0.0574, *wR*2=0.1405 | *R*1=0.0632, *wR*2=0.1365 | *R*1=0.0585, *wR*2=0.1202 | *R*1=0.0588, *wR*2=0.1441 |
| Largest diff. peak and hole (e/Å) | 1.209 −1.812 | 1.324 −1.647 | 1.284 −1.512 | 1.333 −2.140 | 1.305 -1.658 | 1.783 −1.243 |

**Table 2**
Crystal data and structure refinement parameters in experiment S2 ($\lambda$=0.3989 Å) in He medium.

| | | | | | | |
|---|---|---|---|---|---|---|
| Pressure (GPa), medium | 4.53 | 21.36 | 31.35 | 39.92 | 49.12 | 55.18 |
| Unit cell parameters (Å) | *a*=4.9205(9) *c*=13.486(6) | *a*=4.821(1) *c*=13.240(7) | *a*=4.7658(8) *c*=13.134(6) | *a*=4.727(1) *c*=13.065(8) | *a*=4.693(1) *c*=12.977(8) | *a*=4.669(1) *c*=12.929(9) |
| Reflections collected/unique | 135/35 [*R*(int) =0.137] | 140/38 [*R*(int)=0.162] | 134/37 [*R*(int)=0.112] | 136/39 [*R*(int)=0.131] | 110/34 [*R*(int)=0.098] | 117/35 [*R*(int)=0.085] |
| Theta range (deg.) | 3.17 to 16.63 | 3.24 to 17.56 | 3.27 to 17.47 | 3.30 to 17.61 | 3.32 to 17.74 | 3.34 to 17.84 |
| Completeness to max. theta (%) | 34.7 | 34.2 | 35.2 | 37.1 | 32.4 | 33.3 |
| Data/restraints/parameters | 35/0/9 | 38/0/9 | 37/0/9 | 39/0/9 | 34/0/9 | 35/0/9 |
| Goodness-of-fit on $F^2$ | 1.090 | 1.069 | 1.119 | 0.916 | 1.144 | 1.393 |
| Final *R* indices (all data) | *R*1=0.0402, *wR*2=0.0953 | *R*1=0.0352, *wR*2=0.0872 | *R*1=0.0375, *wR*2=0.0585 | *R*1=0.0435, *wR*2=0.0784 | *R*1=0.0405, *wR*2=0.0716 | *R*1=0.0420, *wR*2=0.0989 |
| Largest diff. peak and hole (e/Å) | 0.501 −0.988 | 0.647 −0.620 | 0.781 −0.768 | 0.644 −0.592 | 0.906 −0.872 | 0.845 −0.899 |

The early low pressure single crystal study of $Cr_2O_3$ by Finger and Hazen [5] reported an almost constant behavior of the fractional atomic coordinates, as well as *c/a* ratio with pressure. These results are in excellent agreement with our findings at the lowest pressures. The two highest pressure points of Finger and Hazen [5] for the $X_O$ coordinate deviate from the trend observed in our experiments, but they also have much larger standard deviations, which is understandable considering the low atomic scattering factor of oxygen and the very limited incident beam flux available from the laboratory sealed tube x-ray source.

The higher pressure crystal structure models derived from the earlier powder diffraction experiments [8] suggest a rather peculiar compression mechanism, which is hard to explain in terms of simple interatomic interactions. Oxygen atoms in the shared polyhedral face were suggested to move towards each other upon compression at a rate much higher than the O atoms in the opposite, unshared face. This would result in a fast decrease of the Cr–$O_s$ bonding distance, whereas the Cr–$O_u$ bond length would remain almost constant, creating a very distorted coordination octahedron. At 60 GPa both the 1.77 Å Cr–$O_s$ distance and the 2.2 Å O–$O_{SF}$ distance seem unrealistically short, especially if compared with the remaining bond lengths within the same octahedron. The monoclinic distortion was suggested to have no discontinuous effect on compressional bond length evolution.

Several high-pressure x-ray diffraction studies of the analogous $\alpha$-$Al_2O_3$ have been reported [21–23], but the compression mechanism has not been reliably established to very high pressures. The only available single-crystal study to 31 GPa [23] suggests that the changes of the fractional atomic coordinates are not nearly as dramatic (one order of magnitude smaller slope) as suggested for $Cr_2O_3$ [8]. On the other hand, Rietveld refinements based on a megabar pressure powder diffraction experiments [24] yielded a model with significantly distorted polyhedra, which notably deviates from the single crystal compression trends [23].

The high quality of the single-crystal XRD intensity data obtained in our experiments allowed for refinement of the crystal structure up to a pressure of 55 GPa. Despite the difference in hydrostaticity between Ne and He media used in our experiments S1 and S2 the trends for the pressure evolution of $Z_M$ and $X_O$ obtained from these two experiments are in excellent agreement with each other, as shown in Fig. 3, indicating that the compression mechanism is not strongly dependent on the level of hydrostaticity. Numeric values of the fractional atomic coordinates and equivalent isotropic displacement parameters at different pressures are reported in Tables 3 and 4. The bond compression curves are shown in Fig. 4. The single crystal refinement results differ noticeably from the conclusions of the earlier powder diffraction study [8] and predict that the coordination octahedra become less distorted at high pressure. The quantitative measures of the polyhedral distortion, the angle variance and quadratic elongation [25] both decrease monotonically with pressure as can be seen in Tables 3 and 4. Whereas the structure model does not change fundamentally at 30 GPa, there is a slight change in the slope of the $X_O$ fractional coordinate, which results in small changes of slopes of the Cr–O bonds as well, suggesting that perhaps some new type of interaction comes to play. It is possible that the differences in the compression mechanism obtained from our single-crystal experiments and from the earlier powder diffraction study [8] can be explained by uniaxial stress effects (Ar is significantly less hydrostatic than Ne at 60 GPa), however, it seems more likely that they result from the intrinsic limitations of the powder method and relatively poor resolution of the earlier data. It is also interesting to note that the uniaxial stress-induced peak broadening observed in

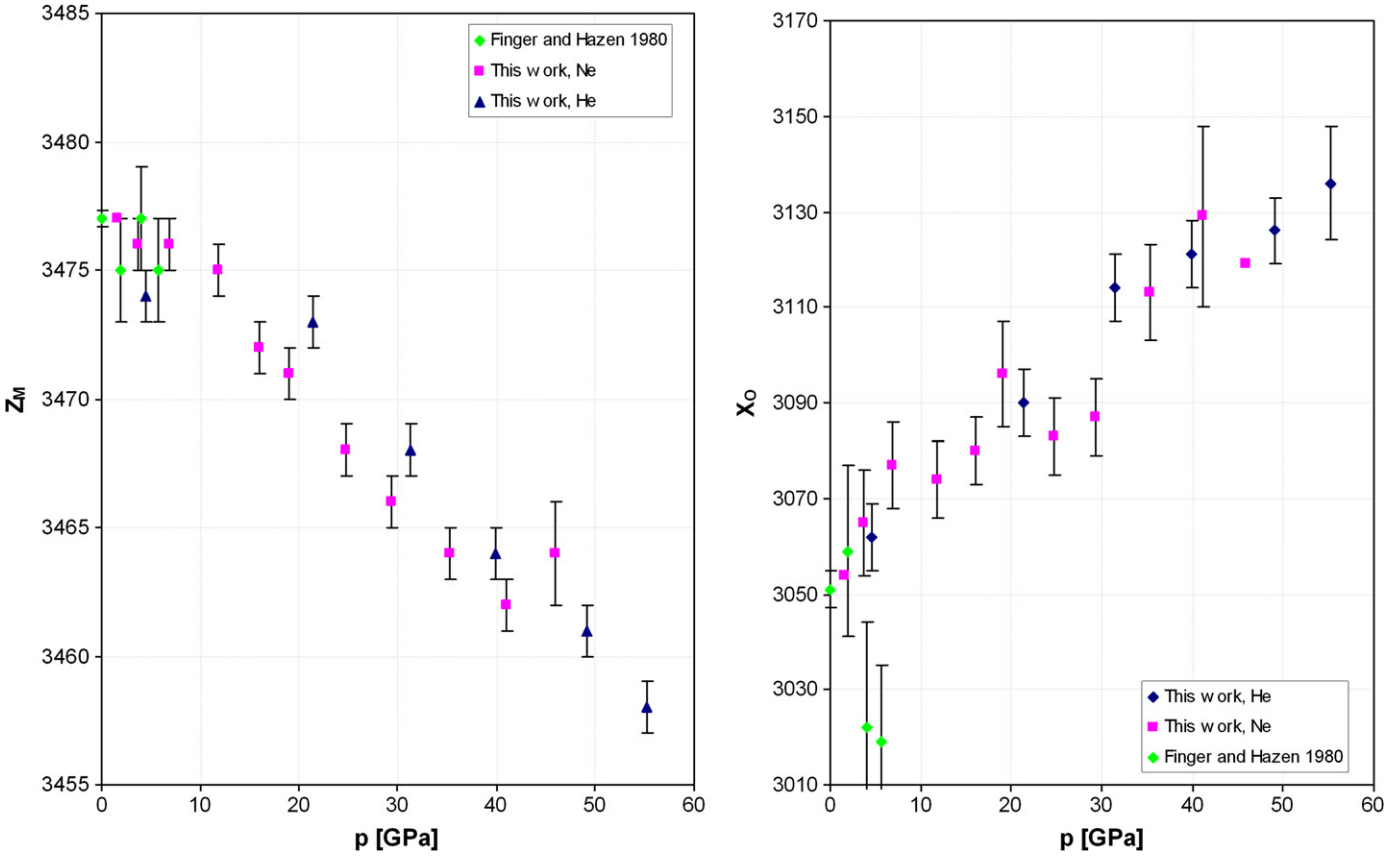


**Fig. 3.** Evolution of fractional atomic coordinates of $Cr^{3+}$ and $O^{2-}$ in $Cr_2O_3$ at high pressure.

**Table 3**
Atomic coordinates and equivalent isotropic displacement parameters (Å$^2$) at selected pressure points in experiment S1. *U*(*eq*) is defined as one-third of the trace of the orthogonalized $U_{ij}$ tensor. Angle variance is a measure of the distortion of the intra-polyhedral bond angles from the ideal polyhedron and quadratic elongation is a measure of the distortion of bond lengths from the ideal polyhedron as defined by Robinson et al. [26].

| | 3.62 GPa | 11.80 GPa | 19.04 GPa | 29.32 GPa | 35.34 GPa | 41.05 GPa |
|---|---|---|---|---|---|---|
| $Z_M$ | 0.3476(1) | 0.3475(1) | 0.3471(1) | 0.3466(1) | 0.3464(1) | 0.3462(1) |
| $X_O$ | 0.3065(11) | 0.3074(8) | 0.3096(11) | 0.3088(8) | 0.3113(8) | 0.3129(10) |
| *M U*(*eq*) | 0.007(2) | 0.006(1) | 0.007(1) | 0.009(1) | 0.008(1) | 0.008(1) |
| *O U*(*eq*) | 0.005(1) | 0.006(1) | 0.006(1) | 0.008(1) | 0.007(1) | 0.006(1) |
| *Polyh. V* (Å$^3$) | 10.233 | 10.123 | 9.828 | 9.589 | 9.289 | 9.172 |
| *Angle variance* | 47.069 | 45.158 | 43.809 | 39.979 | 38.735 | 35.619 |
| *Quadr. elong.* | 1.036 | 1.013 | 1.013 | 1.012 | 1.011 | 1.010 |

**Table 4**
Atomic coordinates and equivalent isotropic displacement parameters (Å$^2$) at selected pressure points in experiment S2. *U*(*eq*) is defined as one-third of the trace of the orthogonalized $U_{ij}$ tensor. Angle variance is a measure of the distortion of the intra-polyhedral bond angles from the ideal polyhedron and quadratic elongation is a measure of the distortion of bond lengths from the ideal polyhedron as defined by Robinson et al. [26].

| | 4.53 GPa | 21.36 GPa | 31.35 GPa | 39.92 GPa | 49.12 GPa | 55.18 GPa |
|---|---|---|---|---|---|---|
| $Z_M$ | 0.3474(1) | 0.3473(1) | 0.3468(1) | 0.3464(1) | 0.3461(1) | 0.3458(1) |
| $X_O$ | 0.3062(7) | 0.3090(7) | 0.3114(7) | 0.3121(7) | 0.3126(7) | 0.3136(12) |
| *M U*(*eq*) | 0.010(2) | 0.006(1) | 0.007(1) | 0.007(1) | 0.009(1) | 0.010(1) |
| *O U*(*eq*) | 0.010(1) | 0.005(1) | 0.006(1) | 0.007(1) | 0.006(2) | 0.009(2) |
| *Polyh. V* (Å$^3$) | 10.064 | 9.523 | 9.264 | 9.075 | 8.891 | 8.781 |
| *Angle variance* | 44.617 | 41.381 | 37.085 | 34.908 | 33.329 | 31.361 |
| *Quadr. elong.* | 1.013 | 1.012 | 1.011 | 1.010 | 1.010 | 1.009 |

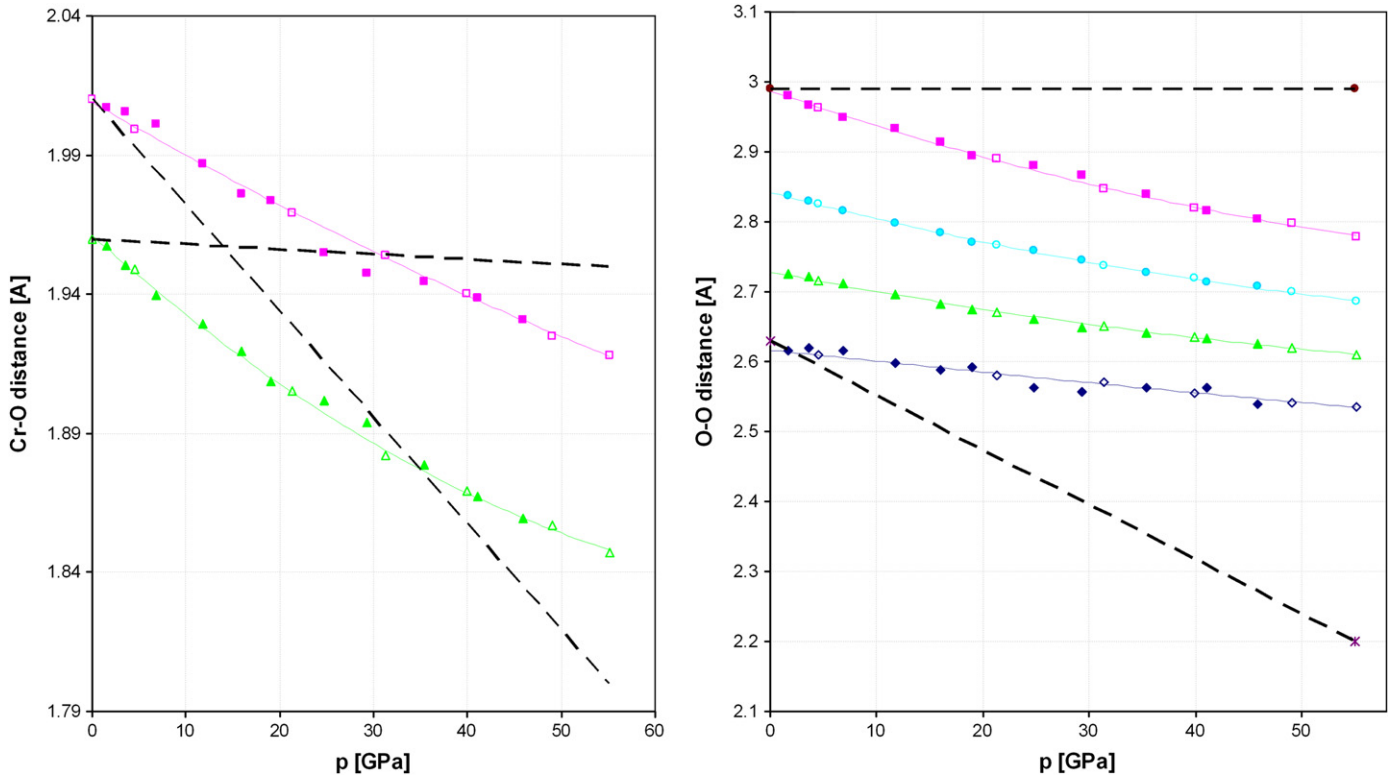


**Fig. 4.** Evolution of Cr–O bonding distances (left panel) and O–O non-bonding interactions (right panel) in $Cr_2O_3$ at high pressure. Filled and open symbols correspond to experiments S1 and S2, respectively. Dashed lines indicate trends proposed by Shim et al. [8]. Experimental errors are smaller than the data point symbols. Solid lines show polynomial fits.

the S1 experiment with Ne medium (illustrated in Fig. 1) was very selective in affecting only certain families of peaks, whereas other peaks, with similar d-spacings remained sharp. It seems reasonable to assume that such an effect, which could have microstructural origin (e.g. formation of antiferrromagnetic microdomains), would be magnified in less hydrostatic pressure media such as alcohol or Ar, and if seen in a powder pattern, could give an impression of symmetry distortion.

### 3.3. Compressibility and possible change in magnetic ordering

The bulk modulus of $Cr_2O_3$ has been reported in several of the earlier studies [5–8], and while there is reasonable general agreement, some differences in the reported values of isothermal bulk modulus $K_{0T}$ exist. The unit cell volume and *c/a* ratio measured in our two single-crystal experiments are compared with the earlier studies in Fig. 5. Considering that each of the earlier experiments was done in a different pressure medium, and some using polycrystalline samples, the general agreement of the volume compression curves is very good. A fit with a third order Birch–Murnaghan equation of state to our experimental data yields $V_0=288.6(2)$ Å$^3$, $K_{0T}=220(4)$ GPa, and $K_0'=4.7(2)$, while a second order fit gives $V_0=288.0(2)$ Å$^3$, $K_{0T}=236(2)$ GPa, with $K_0'$ fixed at 4. The second order fit is in a remarkable agreement with the bulk modulus $K_{0T}=238(4)$ GPa established by Finger and Hazen based on data up to 5.68 GPa, but noticeably smaller than the values of $K_{0T}=259(5)$ and $K_0'=5.0(6)$ reported by Mougin et al. [7].

Since the optical absorption data indicate a possible discontinuity in compression behavior at 30 GPa, we also performed equation of state fits including only volume data below 30 GPa and above 30 GPa. The values of the bulk moduli obtained from second order Birch–Murnaghan fits for these two regions were 228(2) GPa and 249(5) GPa, with $K_0'$ fixed at 4, indicating that the optical transition may be associated with increase in the incompressibility.

It has been previously suggested that the compressibility of the $CrO_6$ polyhedra in ruby is lower than the compressibility of the unit cell volume, but the effect was attributed to the fact that $Cr^{3+}$, as substituting ion, has a larger ionic radius than $Al^{3+}$ [26]. Duclos et al. [27] demonstrated that assuming a 6% difference in polyhedral and bulk compressibility can sufficiently explain the deviation from the cubic point charge model observed for ruby up to 35 GPa. Polyhedral volumes calculated for our high-pressure structure models are listed in Tables 3 and 4, show a very linear dependence on the bulk volume (illustrated in the inset of Fig. 8b) and indicate a 6.7% lower compressibility than the bulk volume. This observation suggests that the $CrO_6$ polyhedral compressibility offset in ruby is intrinsic to the compression mechanism of $Cr_2O_3$ in the corundum structure rather, than being related to the mismatch of the ionic radius of the substituting ion.

No identifiable discontinuity in volume or slope of the $V(p)$ was found at pressures corresponding to the two sample color changes observed. Interestingly, however, while most earlier experimental studies reported essentially constant pressure behavior of *c/a*, we see a change in the trend occurring above 15 GPa (the same pressure at which the color change from green to red occurs). The axial ratio, initially constant at pressures below 15 GPa, starts noticeably increasing above that point (shown in the lower inset of Fig. 5). The change in the *c/a* trend is clearly a result of a decrease in compressibility along the 0 0 1 direction (illustrated in the upper inset of Fig. 5), and indicates new type of interactions coming into play. First principles calculations [13] strongly suggest that the pressure-dependence of the *c/a* ratio should be different for different magnetic structures. The PM phase is predicted to show an almost constant behavior of *c/a*, consistent with our observations up to 15 GPa. A PM→AFM transition should be accompanied by change to positive pressure gradient of *c/a* ratio, as shown in the lower insert to Fig. 5. The predicted slope of *c/a* for AFM state is slightly steeper than the observed trend above 15 GPa, but the general agreement seems convincing.

It is also interesting to note that the $Z_M$ atomic coordinate shows two different pressure-trends coinciding with the discontinuity in the *c/a* behavior. Below 15 GPa $Z_M$ is almost constant,

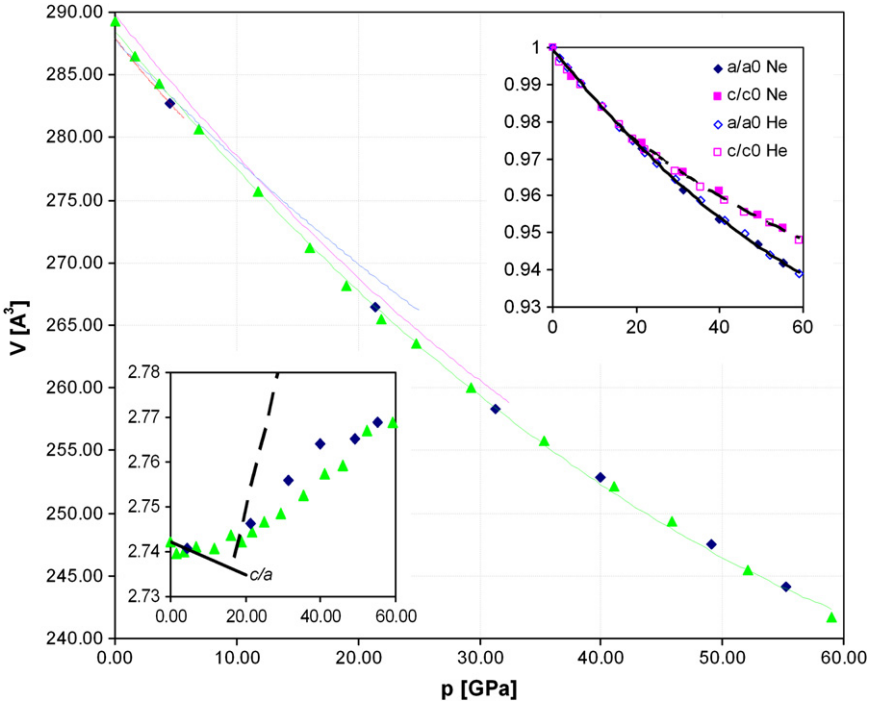


**Fig. 5.** Pressure evolution of the unit cell volume, axial ratio (lower insert) and normalized unit cell parameters (upper insert) of $Cr_2O_3$. Red, blue and purple curves correspond to equations of state determined by Finger and Hazen [5]. Mougin et al. [7], and Rekhi et al. [6], respectively. Data of Shim et al. [8] is generally consistent with Mougin et al. [7] up to 30 GPa, but is omitted in this comparison because as many as four different fits resulting in very different $V(p)$ were presented. Green curve shows quadratic fit. Solid line in the lower insert shows the first principles *c/a* trend for the PM phase, while dashed line is the trend for AFM phase [14]. Experimental errors are smaller than the data point symbols. (For interpretation of the references to color in this figure legend, the reader is referred to the web version of this article.)

while it starts noticeably decreasing above that point (as illustrated in Fig. 3). The nearest-neighbor Cr–Cr distances are aligned along the 0 0 1 crystallographic direction, and decrease with decreasing $Z_M$.

In the context of a possible magnetic transition at 15 GPa it is important to note that uniaxial stress was demonstrated to have a significant effect on $\partial T_N/\partial p$. Alberts and Boyens [28] showed that uniaxial stress applied along the [0 0 1] direction would shift $T_N$ to lower temperatures, whereas stress applied along the [1 0 0] direction would increase $T_N$. This kind of effect would create a big difference between high-pressure experiments involving single crystal and polycrystalline samples in quasi-hydrostatic environments. The single-crystal sample has a well defined orientation with respect to the anisotropic stress field, and $T_N$ is affected by the uniaxial stress component in a uniform way. In the case of polycrystalline samples differently oriented micrograins would have their $T_N$ affected in different ways by the uniaxial component, most likely resulting in a coexistence of two populations of grains in different magnetic states over a wide range of pressures, which could manifest itself in splitting of diffraction peaks, reminiscent of symmetry distortion. Perhaps this effect could account for the indication of the monoclinic distortion in earlier powder diffraction experiments.

### 3.4. Electronic absorption spectra

Hydrostatic compression of α-$Cr_2O_3$ induces clearly visible changes in the color of the sample, as illustrated in Fig. 6. The sample transforms from green through red (above 15 GPa), to orange (above 30 GPa). This phenomenon, known as a barochromic (or piezochromic) effect, often occurs in transition metal compounds unrelated to structural transitions [29], and can be quantitatively characterized by measuring changes in the electronic absorption spectra. The color of $Cr^{3+}$-containing corundum crystals is determined by two broad absorption bands, which are attributed to electronic transitions between quartet states $^4A_{2g}\rightarrow{}^4T_{2g}(F)$ and $^4A_2\rightarrow{}^4T_{1g}(F)$. There are two important characteristics of the crystal field that can be derived from the energies

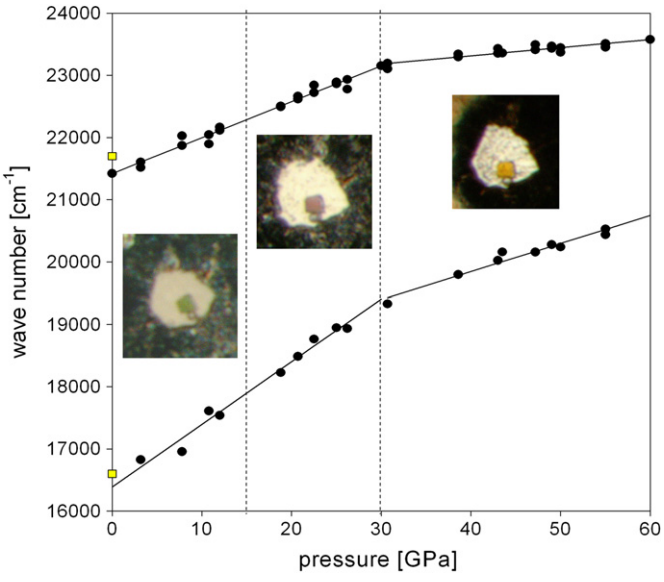


**Fig. 6.** Pressure evolution of the two absorption bands in $Cr_2O_3$. Inserts show appearance of the single-crystal sample in transmitted light at different stages of compression. Vertical dashed lines indicate pressures at which the color changes occur. (For interpretation of the references to color in this figure, the reader is referred to the web version of this article.)

of the two absorption bands: the crystal field splitting $\Delta = 10Dq$ and the Racah $B$ parameter. Because of electron–phonon coupling, the excited states are modified by lattice strain, and therefore the energies of the two quartet bands are affected by changes in the unit cell parameters.

In order to quantify the observed changes in the sample color we performed optical absorption spectra measurements using a single crystal sample immersed in Ne pressure medium in a diamond anvil cell, in the pressure range of 0–60 GPa. At every pressure point a pair of spectra, one going through the α-$Cr_2O_3$ crystal, and a second, going through a region of the gasket filled only with Ne medium were recorded. Absorbance was calculated as

$$A = \frac{1}{x}\log_{10}\frac{I_0}{I}, \tag{1}$$

where $x$ is the sample thickness, $I$ is the intensity of light transmitted through the sample and $I_0$ is the incident light intensity (in our measurements approximated by the intensity of light passed through the pressure medium in the gasket hole). Examples of the absorbance spectra at increasing pressure are shown in Fig. 7. All spectra were analyzed by fitting the two absorption bands with Voigt functions. Results of peak fitting are summarized in Fig. 8. Changes in the sample thickness accompanying compression, which do not affect the positions of the absorption peaks were ignored. The values of energy of the quartet transitions obtained in our experiments extrapolated to ambient pressure are in excellent agreement with values reported by Poole [30]. Both band energies increase with pressure, as previously observed for ruby [27]. The first color change observed at 15 GPa does not seem to be associated with any discontinuities in absorption band positions, intensities or widths and its nature can be attributed to the artificial discontinuity in the dispersion of the human eye sensitivity [29]. There is, however, a significant change in the slope of both curves describing the evolution of band energy with pressure, located at 30 GPa, where the second color change, to orange, was observed. Similar discontinuities were observed in the evolution of band widths and intensities. It should be emphasized that in both diffraction experiments S1 and S2 the same two color changes were observed (at the same pressures) as in the optical absorption measurement, suggesting that the optical transitions seen in the latter are not induced by the Ne nonhydrostaticity. Furthermore, the results of Klotz et al. [16] show no discontinuity of the pressure-evolution of $\sigma$ for Ne at 30 GPa.

A spectral parameter, which is commonly used to describe the covalency of the bonds in transition metal crystals, is the Racah $B$ parameter, which can be calculated according to the following formula [31]:

$$B = \frac{1}{3}\frac{(2\upsilon_1-\upsilon_2)(\upsilon_2-\upsilon_1)}{9\upsilon_1-5\upsilon_2}, \tag{2}$$

where $\upsilon_1$ and $\upsilon_2$ are energies of the $^4A_{2g}\rightarrow{}^4T_{2g}$ and $^4A_{2g}\rightarrow{}^4T_{1g}$ transitions, respectively. Duclos et al. [27] measured the pressure evolution of the electronic absorption spectrum of ruby to 35 GPa and found that the crystal field splitting parameter $10Dq$ increases linearly with pressure, whereas $B$ exhibits a linear decrease, corresponding to a gradual increase in bond covalency. Similar behavior was observed for other inorganic crystals containing $Cr^{3+}$ in octahedral coordination [29,31]. Our results for $Cr_2O_3$ show an increase in $10Dq$, with a discontinuous slope change at 30 GPa. The compression behavior of $B$ shows a linear decrease, with a small change in the slope around 30 GPa, as shown in Fig. 8a.

In the simple approach to crystal field theory the ligands are considered as point-charges $-Ze$, residing at a distance $a$ from the

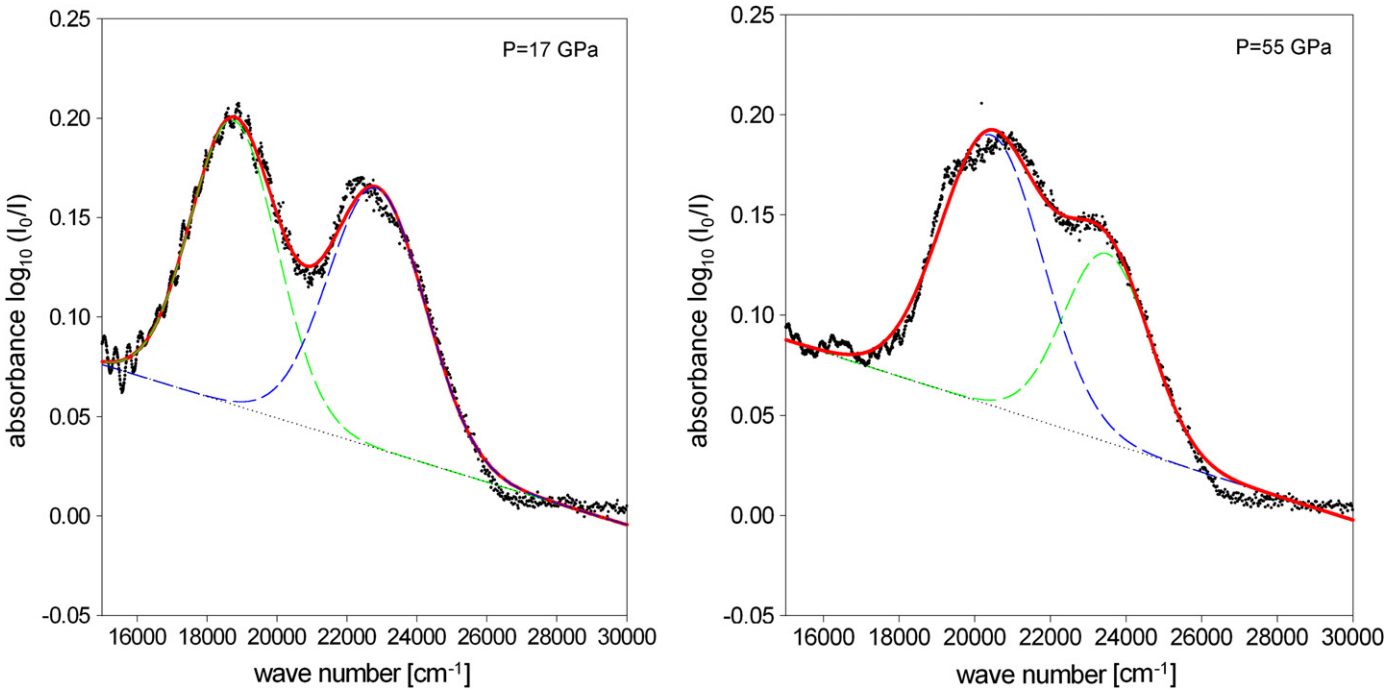


**Fig. 7.** Absorbance spectra of $Cr_2O_3$ measured on a single-crystal sample in Ne pressure medium at different pressures. Dashed curves show fitted profiles of the two spectral components of the spectrum.

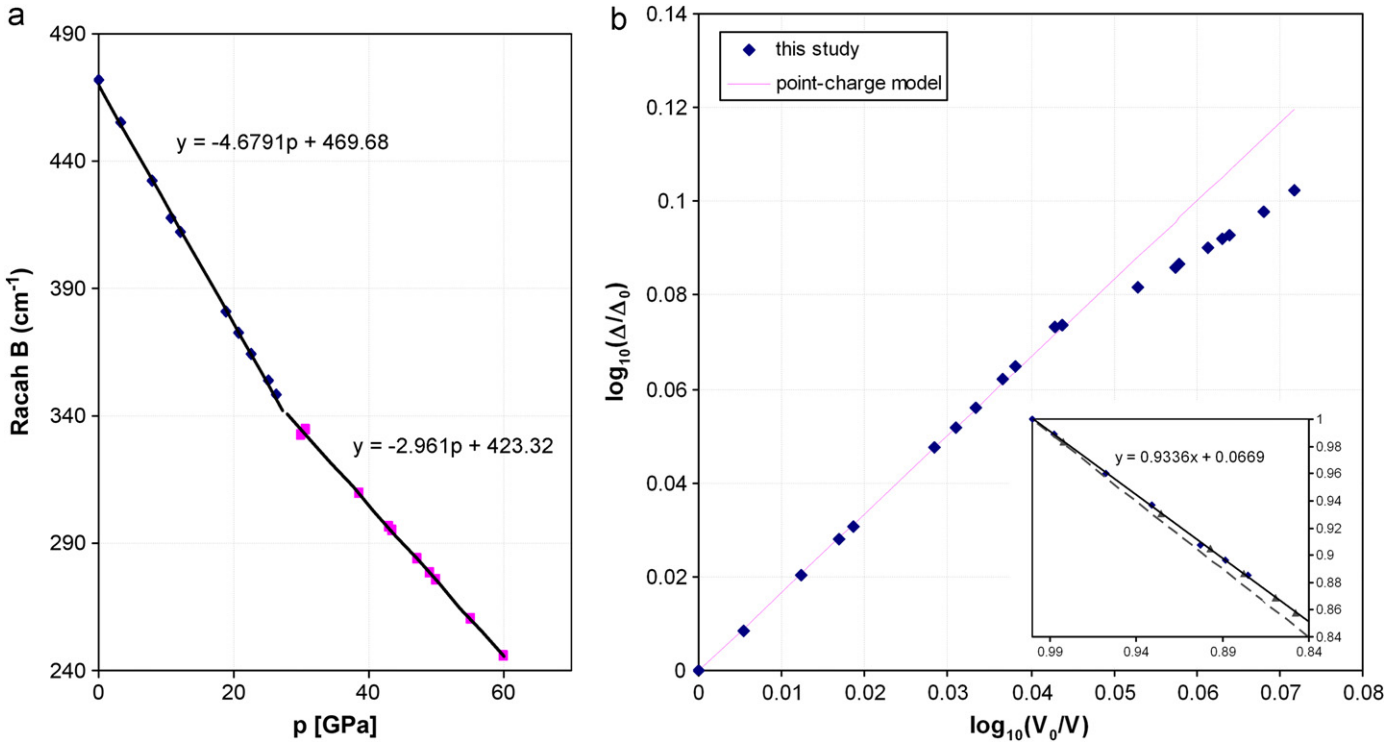


**Fig. 8.** (a) Pressure-evolution of the Racah B parameter and (b) verification of the cubic point-charge model approximation. The departure from the point-charge model trend occurs at 30 GPa and coincides with the second color change. Insert in figure b) shows evolution of the normalized polyhedral volume as a function of unit cell volume. The dashed line in the insert is the $y=x$ reference. $CrO_6$ polyhedra are 6.7% less compressible that the whole unit cell. No discontinuity in polyhedral volume is observed at 30 GPa. (For interpretation of the references to color in this figure, the reader is referred to the web version of this article.)

central atom. According to this approximation the crystal field splitting can be calculated as:

$$\Delta = b\frac{Ze\langle r^4\rangle_{3d}}{a^5}, \tag{3}$$

where $b$ is a constant factor, $Z$ is the atomic number, $e$ is the electron charge, and $\langle r^4\rangle_{3d}$ is the $Cr^{3+}$ $3d$ orbital function. Since $Z$, $e$, and the orbital function are in principle not expected to vary with pressure, one of the consequences of the point-charge approximation (PCA) is that $\Delta$ should scale with $V^{-5/3}$.

The departures from the PCA dependence are usually attributed to one of the following factors: (i) multipole departure from point-type charge distribution of ligands [32], (ii) scaling of electronic charge and nuclear charge number with volume [33], (iii) interactions between $^4T_2$ and $^2T_2$ states (anticrossing theory) [34] or (iv) differences in volume and octahedral compression in solid solutions [27]. The dependence between the reduced crystal field splitting and reduced polyhedral volume determined in our experiments for $Cr_2O_3$ up to 60 GPa is presented in Fig. 8b. The PCA explains the observed dependence perfectly up to the pressure of 30 GPa, corresponding to the change of color from red to orange. Above the transition pressure the dependence is still linear, but exhibits a very different slope. Similar departure from the point-charge model has been reported for ruby [27], however, while in the case of ruby the departure manifests itself significantly also only at higher pressure, it was approximated by a single linear trend and explained in terms of difference in the bulk and $CrO_6$ polyhedral compressibility. In the case of $Cr_2O_3$ the departure from PCA is clearly more discontinuous than in ruby (which might be related to the dilution of Cr atoms in the latter). Based on the continuous polyhedral compression trend (inset of Fig. 8b) this behavior cannot be attributed to a discontinuity in polyhedral volume compression, but instead seems related to charge density redistribution or discontinuous change in the $^4T_2$ and $^2T_2$ interactions. The change in the Cr–O bond covalency indicated by the change of slope of $B(p)$ seems to be consistent with the hypothesis of charge transfer.

## 4. Conclusions

Combined synchrotron x-ray diffraction experiments and optical absorption measurements with synthetic single-crystal $Cr_2O_3$ reveal that the corundum-type structure is preserved to at least 55 GPa, and no indication of earlier reported monoclinic distortion has been found.

The compression mechanism revealed by the diffraction experiment is quite different from the earlier reported bond compression trends based on polycrystalline diffraction and Rietveld analysis and shows that the coordination environment of the $Cr^{3+}$ ions is not significantly distorted up to 55 GPa.

The first color change from green to red has been found not to be associated with discontinuities in $10Dq$ or $B$ evolution, but does coincide with a change in the $c/a$ ratio behavior, which starts noticeably increasing above 15 GPa and may be associated with a change in magnetic ordering.

The second change in the sample color, occurring at approximately 30 GPa does not seem to coincide with any significant structural distortion, but its spectral signature indicates departure from the point charge model above 30 GPa most likely related to charge density redistribution or discontinuous change in the $^4T_2$ and $^2T_2$ interactions.

## Acknowledgments

The authors would like to thank J. Stubbs (Univ. of Chicago) and Y. Feng (ANL) for critical reading of the manuscript and useful suggestions. We are also grateful to Prof. R.T. Downs and another anonymous reviewer for valuable comments and suggestions. This project was supported by a grant from the MRI Program, Division of Materials Research, National Science Foundation (NSF-DMR-0521179). Part of this work was performed at GSECARS (Sector 13), Advanced Photon Source (APS), Argonne National Laboratory. GSECARS is supported by the National Science Foundation, the U.S. Department of Energy, the W.M Keck Foundation, the U.S. Department of Agriculture and the State of Illinois. Portions of this work were performed at HPCAT (Sector 16), Advanced Photon Source (APS), Argonne National Laboratory. HPCAT is supported by CIW, CDAC, UNLV and LLNL through funding from DOE-NNSA, DOE-BES and NSF. APS is supported by DOE-BES, under Contract no. DE-AC02-06CH11357.

## References

[1] H.K. Mao, J. Xu, P.M. Bell, J. Geophys. Res. 91 (1986) 4673–4676.
[2] S.D. Jacobsen, et al., Am. Mineral. 93 (2008) 1823–1828.
[3] H.J. Lewis, H.G. Drickamer, J. Phys. Chem. 45 (1966) 224.
[4] Y. Sato, S. Akimoto, J. Appl. Phys. 50 (1979) 5285.
[5] L.W. Finger, R.M. Hazen, J. Appl. Phys. 51 (1980) 5362–5367.
[6] S. Rekhi, et al., J. Alloys Compd. (2000) 16–20302 (2000) 16–20.
[7] J. Mougin, T.L. Bihan, G. Lucazeau, J. Phys. Chem. Solids 62 (2001) 553–563.
[8] S.H. Shim, et al., Phys. Rev. B69 (2004) 144107.
[9] P.D. Dernier, M. Marezio, Phys. Rev. B2 (1970) 3771–3776.
[10] T.G. Worlton, R.M. Brugger, R.B. Bennion, Phys. Chem. Solids 29 (1968) 435–438.
[11] G. Gorodetsky, R.M. Hornereich, S. Shtrikman, Phys. Rev. Lett. 31 (1973) 938–940.
[12] M. Catti, et al., J. Phys. Chem. Solids 57 (1996) 1735–1741.
[13] A.Y. Dobin, W. Duan, R.M. Wentzcovitch, Phys. Rev. B62 (2000) 11997–12000.
[14] M.L. Rivers, et al., High Pressure Res. 28 (2008) 273–292.
[15] P. Dera, GSE_ADA data analysis program for monochromatic single crystal diffraction with area detector, GSECARS, Chicago, IL, 2007.
[16] S. Klotz, et al., J. Phys. D: Appl. Phys. 42 (2009) 075413.
[17] G.M. Sheldrick, Acta Cryst. A64 (2008) 112–122.
[18] D.B. McWhan, J.P. Remeika, Phys. Rev. B2 (1970) 3734–3750.
[19] D.B. McWhan, et al., Phys. Rev. B7 (1973) 1920–1926.
[20] S.A. Carter, et al., Phys. Rev. B49 (1994) 7898–7903.
[21] H. D′Amour, et al., J. Appl. Phys. 49 (1978) 4411–4416.
[22] L.W. Finger, R.M. Hazen, J. Appl. Phys. 49 (1978) 5823–5826.
[23] J. Kim-Zajonz, S. Werner, H. Schulz, Z. Kristallogr. 214 (1999) 331–336.
[24] J.-F. Lin, et al., Nat. Mater. 3 (2004) 389–393.
[25] K. Robinson, G.V. Gibbs, P.H. Ribbe, Science (1971) 567–570172 (1971) 567–570.
[26] T. Goto, T.J. Ahrens, G.R. Rossman, Phys. Chem. Miner. 4 (1979) 253–263.
[27] S.J. Duclos, Y.K. Vohra, A.L. Ruoff, Phys. Rev. B41 (1990) 5372–5381.
[28] H.L. Alberts, J.C.A. Boeyens, J. Magn. Magn. Mater. 2 (1976) 327–333.
[29] M.N. Taran, K. Langer, M. Koch-Muller, Phys. Chem. Miner. 35 (2008) 175–177.
[30] C.P. Poole, J. Phys. Chem. Solids 25 (1964) 1169–1182.
[31] R.M. Abu-Eid, R.G. Burns, Am. Mineral. 61 (1976) 391–397.
[32] S. Sugano, Y. Tanabe, H. Kamimura, Multiplets of Transition-Metal Ions in Crystals, Academic Press, New York, 1970.
[33] R.G. Munro, J. Chem. Phys. 67 (1977) 3146–3150.
[34] J.H. Eggert, K.A. Goettel, I.F. Silvera, Phys. Rev. B40 (1989) 5724–5732.